Variable Inductor Based Bidirectional DC–DC Converter for Electric Vehicles

Mebrahtom Woldelibanos Beraki, *Student Member, IEEE*, João Pedro F. Trovão [ID] , *Member, IEEE*,
Marina S. Perdigão, *Member, IEEE*, and Maxime R. Dubois, *Member, IEEE*

Abstract—This paper presents the feasibility study of variable inductor (VI)-based bidirectional dc–dc converter for applications with a wide range of load variations such as electric vehicles. An additional winding is introduced to the conventional power inductor to inject a control current for adjusting the permeability of magnetic cores. This has significant merits in controlling the current ripple and enhancing the current handling capability of power inductors, thereby reducing the size of magnetic components and improving the performance. For current values, twice and three times the rated current, the current ripple is reduced by 40.90 % and 36.10 %, respectively. Nonetheless, this device requires a precisely controlled dc-current. As such, a small current controlled, low-power and low-cost buck converter is built to power up the auxiliary winding. To improve the reliability and robustness of the VI, an integrated closed loop control that enables the control of the main converter and the auxiliary converter is also implemented and tested in real time to test the viability of the VI.

Index Terms—Bidirectional DC-DC converter, electric vehicle, magnetic core, ripple control, traction, variable inductor.

I. INTRODUCTION

IN TRACTION systems, energy sources should be connected to the motor drive by efficient and suitable power electronics converters. These converters are vital in adapting the voltage levels, managing the power flow and provide better performances [1]–[3]. Their sizing, selection and design is very critical, since they are required to have smaller size, higher efficiency, higher power density and enhanced overall performance [4]. The power inductor and the dc-link capacitor are key components that dominate the size and dynamic performance of power electronic converters [5]. Due to wide range of load variations in traction applications, the selection of these components, particularly the power inductor requires a meticulous attention. This is mainly due to the core material limitations, losses and its impact on the overall performance [6]–[8]. Conventionally, this component is selected to meet the ripple specifications under all operating conditions. Nonetheless, in applications where there are wide range of dynamic load variations and with multiple kind of energy storage systems, such as electric vehicles (EVs), the transient currents during acceleration and regenerative braking may reach very high values. Selecting power inductors to meet the high transient currents will lead to bulky and heavy power inductors. This increase the size and weight of power electronic converters. Larger power electronic converters, limit the space for energy sources, thereby restricting the autonomy of EVs. Therefore, it is vital to scale down the size of passive components in order to reduce the overall size of these converters. This has motivated the adoption of numerous studies [4], [6], [9]. Several methods such as the development of new materials, winding configurations, assembly techniques, increasing the switching frequency, interleaving techniques, the use of coupling inductors and the use of permanent magnets have been proposed and explored in recent literature [6], [7], [10], [11].

Magnetic-based solutions have been presented in recent literature; integrated winding coupled inductors have been used to reduce the size and volume of the magnetic material. However, they have higher switching losses due to close coupling and stray capacitance [11]. Furthermore, interleaving technique has been successfully used to reduce the size of passive components, reducing the input current ripple, improving the efficiency and dynamic performance, reliability and modularity [12]. Nevertheless, it requires higher number of components count and current balancing control which complicate the control circuitry [13].

Power inductors in interleaved converters can be also integrated in a single core with specific coupling methods in order to reduce the size of the magnetic core and improve the performance [14], [15]. However, there is a considerable leakage inductance due to the non-ideal coupling of the coupled inductors which results in high voltage spikes and parasitic ringing, which require additional circuitry to compensate this effect. The use of permanent magnets to partially cancel the magnetic fluxes in magnetic cores have been also used to enhance the saturation current and reduce the size of power inductors [7]. Even though this solution provides remarkable improvement

M. W. Beraki and M. R. Dubois are with the Department of Electrical Engineering and Computer Engineering, Université de Sherbrooke, QC J1K 2R1, Canada (e-mail: Mebrahtom.Beraki@USherbrooke.ca; Maxime. Dubois@USherbrooke.ca).

J. P. F. Trovão is with the Department of Electrical Engineering and Computer Engineering, Université de Sherbrooke, Sherbrooke, QC J1K 2R1, Canada, and also with the Institute for Systems and Computers Engineering at Coimbra, Coimbra P-3000-033, Portugal (e-mail: Joao.Trovao@USherbrooke.ca).

M. S. Perdigão is with the Instituto de Telecomunicações, Coimbra 3030-290, Portugal, and also with the Polytechnic Institute of Coimbra, Coimbra 3030-290, Portugal (e-mail: perdigao@isec.pt).
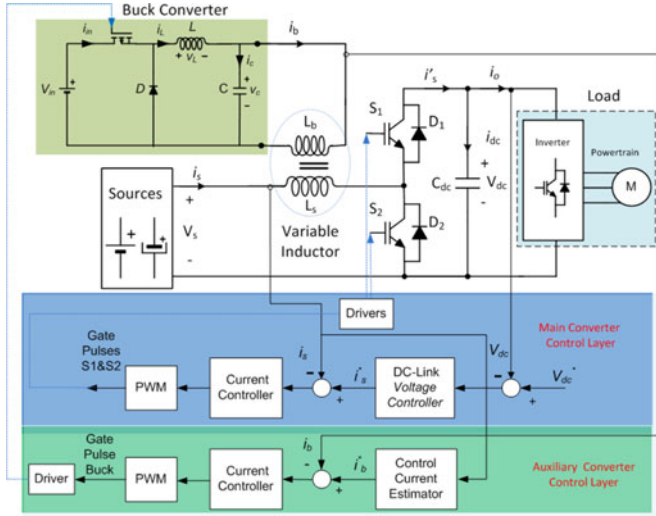
Fig. 1. Schematic Diagram of VI-based bidirectional converter and its control structure.

Fig. 2. B-H curve for illustrating the operation of VI.

in doubling the saturation current, its control flexibility is limited.

In this paper, a current controlled magnetic device, the so-called variable inductor (VI) is introduced into a half-bridge bidirectional DC-DC converter (as shown in Fig. 1) to enhance the inductor flux density capability. By feeding the auxiliary winding with a controlled dc-current in closed loop operation, it is possible to detect high current load demands and regulate the saturation level of the core. For this, a power control layer and an additional converter are designed and implemented. The auxiliary converter used in this study is smaller and has less number of components compared to the H-bridge [10] and forward [16] converters proposed in literature. Besides improving the current handling capability of the power inductor by effectively controlling the reluctance of the magnetic core, the VI will also act as a current ripple regulator. Furthermore, with faster controllers, by forcing the power inductor to saturation, faster transient performances can be obtained [10]. This points out another salient advantage of the VI.

This paper is organized in five sections. The introduction is presented in Section I. Section II introduces the VI-concept, including its operating principles, its application in ripple control, the selected topology and its configuration. The general overview of the studied system and the design of the controllers for the main and auxiliary converters are provided in Section III. Section IV presents the experimental system and the results. Finally, the concluding remarks and future works are presented in Section V.

II. VARIABLE INDUCTOR CONCEPT

A. Operating Principle and Ripple Control

A VI is a dc-current controlled, multiple winding inductor realized in various geometries and magnetic cores [17]–[19]. It consists of a main winding and an auxiliary winding where the dc-control current is applied to adjust the reluctance level of the
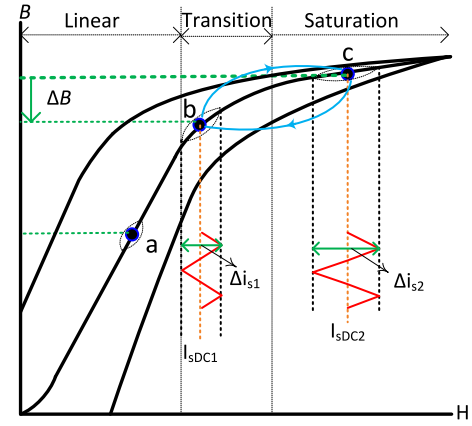
core. The controlled current in the auxiliary winding alters the magnetic flux density of the core and adjusts the operating point in the $B - H$ curve.

To illustrate the fundamental concepts involved a classical $B - H$ curve is revealed in Fig. 2.

In the proposed bidirectional converter, a C-Class chopper, the amount of the inductor current ripple is given by:

$$\Delta i_s = \frac{V_s D_s T_s}{L_s} \quad (1)$$

where V_s is the source voltage, D_s is the duty cycle (the ratio of the on-time to the switching period), L_s is the inductance of the power inductor and Δi_s is the current ripple. As shown in (1), the amount of current ripple is inversely proportional to the inductance of the power inductor. If the power inductor is operated in the saturation region of the $B - H$ curve, its inductance will fall due to the reduction in the permeability of the material. This will influence the dynamic performance of the converter as well as the expected levels of current ripple and losses.

Referring to Fig. 2, three different load conditions are considered, a – light load, b – transition load (which corresponds to an average current level (I_{sDC1}), in the power converter) and c – heavy load (corresponding to a higher average current level (I_{sDC2}). In point a, the power inductor operates in the linear region, hence there is no effect on the level of the current ripple, since the value of the inductance remains constant. By pushing the operating point to b and c, the core enters in the transition and saturation regions. Consequently, the inductance of the power inductor will be reduced. As a result, the current ripple will increase. The increase in the current ripple and reduction of the inductance leads to higher rms current leading to higher losses and heating in the power converter and switches.

With a control current injected into the VI, the operating point c, at heavy-load, can be adjusted. By cancelling part of the main winding flux density, the operating point can be moved down to the transition region from point c to point b as shown by the blue arrow. In fact, resulting in inductance, which is higher than the inductance at point c, maintaining the level of the current ripple at reasonable values. For two operating points b and c, the projected waveforms are to illustrate the effect of the change in
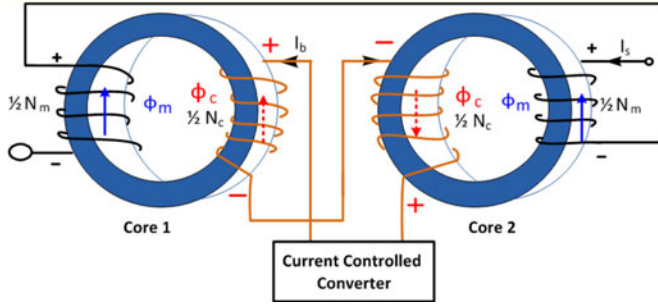
Fig. 3.   Schematic diagram of VI-Prototype with its Control Converter.

TABLE I
SPECIFICATIONS THE VI-PROTOTYPE

Ferrite core Toroid R 102 × 65.8 × 15.0 (mm) with Epoxy coating	
Core material	N87 from EPOCS
Main winding wire gauge	4.17 mm^2
Bias winding gauge	0.65 mm^2
Main winding number of turns	28
Auxiliary winding number of turns	360
Total Volume of VI	0.273 dm^3

inductance with increase of current and its impact in the current ripple. I_{sDC2} is greater than I_{sDC1} consequently, Δi_{S2} is greater than Δi_{S1}. In conclusion, operation in the saturation leads to the higher current ripples and more losses.

B. VI Topology for Bidirectional Operation

The main challenge for the VI structure is the forced bidirectional operation. It must operate in motoring or regenerative braking modes. Typically, VIs are built with a main and an additional winding, with mandatory decoupling between the two. The main winding corresponds to the power inductor and the auxiliary winding is connected to a current controlled DC-DC converter. This auxiliary converter must be small and a low-power to avoid any significant additional losses to the whole system.

Fig. 3 depicts the schematic diagram of the studied VI. It is realized by two sets of windings, the main winding and the auxiliary winding wound into two magnetically decoupled magnetic cores. The two windings are wound on two toroidal ferrite cores, each made by stacking of two cores.

Both the main winding and auxiliary winding number of turns are equally divided into the two toroidal cores. The main winding in the core 1 and in core 2 are electrically connected in series. Similarly, the auxiliary windings in the two cores are connected in series. However, to cancel the amount of reflected voltages from these windings to the main windings, they are wound in such way that the net induced voltage is nil. This accounts for the required decoupling action.

Fig. 3 shows the directions of the fluxes: the red arrow represents the flux imposed by the current flowing in the auxiliary winding and the blue one represents the flux imposed by the main winding. In core 1, the magnetic flux from the main winding and the magnetic flux from the auxiliary winding partially cancel each other, whilst in core 2, the two fluxes add up. In core 1, the cancelation of the flux moves the operating point of the core to the linear/transition region while in core 2, the additive flux forces the magnetic core to operate in the saturation region. Nonetheless, this configuration has better saturation regulation and ripple current control in comparison to the same configuration with no control current in the auxiliary winding. Also, as the main windings are electrically connected in series, the total inductance will be the sum of each individual inductances. Therefore, with this approach the effective inductance

can be regulated. It has to be noted that the auxiliary winding is idle during the levels of current less than the saturation current of the power inductor. However, for currents greater or equal to the saturation current the control current is injected in order to enable the partial saturation operation of the power inductor.

In order to have minimum impact of the auxiliary winding on the overall efficiency of the bidirectional converter, the auxiliary winding number of turns are made much higher than the main winding number of turns. Besides the gauge of the main winding is about 6.5 times larger than the auxiliary winding wire gauge. The specifications of the studied VI-prototype are detailed in Table I.

To exploit the merits of the VI in controlling the current ripple and improving the current handling capability of magnetic cores, the auxiliary winding current has to be precisely controlled. To do so, a mathematical relationship between the auxiliary winding and main winding currents is vital. As such, based on the open loop first studies, the relationship between the two currents is obtained using curve fitting. This is further presented in Section IV and the curve that relates the auxiliary winding current and the main current is revealed in Fig. 5.

III. SYSTEM DESCRIPTION

In order to test the proposed solution, a bidirectional converter and a VI were designed and built. The converter was designed in such away; it is capable of sustaining load changes with stable dc-link operation. The VI was designed to easily operate in conditions correspondent to heavy loads, meaning it would saturate relatively fast. The overall schematic diagram of the system used in this study is depicted in Fig. 1. The bidirectional converter is a C-Class DC chopper, which enables two-way flow of current, consisting of energy sources (such as batteries or supercapacitors), a variable inductor, two active switches (IGBTs) and a dc-link capacitor. The auxiliary converter is a buck-type used for controlling the current of the auxiliary winding to regulate the effective inductance of VI.

The energy storage system supplies power to the traction system, and the bidirectional converter acts as a boost converter to step-up the supply voltage to the dc-link voltage during normal operation and hard acceleration. Whilst, during regenerative braking it behaves as a step-down converter to charge the storage systems. The conventional saturating power inductor is replaced by a dc-current controlled VI. The dc-current, in the auxiliary winding of the VI is used to regulate the effective inductance of

TABLE II
MAIN CONVERTER DESIGN SPECIFICATIONS

	Variable	Value	Unit
Nominal input voltage	V_s	12	V
Nominal output voltage	V_{dc}	24	V
Inductor current ripple	Δi_s	45%	
Rated inductor current	I_s	6	A
Output voltage ripple	Δv_{dc}	10%	
PWM switching frequency	f_{sw}	20	kHz

TABLE III
AUXILIARY (BUCK) CONVERTER DESIGN SPECIFICATIONS

	Variable	Value	Unit
Nominal Input Voltage	V_{in}	12	V
Nominal output voltage	V_o	3	V
Current ripple	Δi_b	5%	
Voltage ripple	Δv_o	10%	
PWM switching frequency	f_{sw}	20	kHz

the inductor passive component during higher current demands in hard acceleration and regenerative braking of EV.

Fig. 1 also shows the required control layers to operate and test this solution. The main converter control layer consists of a dc-link controller and a current controller for the bidirectional DC-DC converter. The dc-link voltage controller is used to keep the dc-link voltage within the limit so that there is stable voltage to be delivered to the load and prevent current ripple propagation to the source. The auxiliary converter control layer consists of a current controller for auxiliary converter and a reference current estimator, which determines the reference current for the auxiliary winding control current.

A. Main Converter Control Design

The main converter is a C-Class DC chopper with bidirectional current flow capability. The specifications of the main winding converter are shown in Table II.

The average model of the converter can be derived from the dynamic equations of the converter in a complete switching period.

$$L_s \frac{di_s(t)}{dt} = v_s(t) - (1 - d_s(t)) v_{dc}(t) \quad (2)$$

$$C_{dc} \frac{dv_{dc}(t)}{dt} = i'_s(t) - i_o(t) \quad (3)$$

where v_s, d_s, v_{dc}, i_s, i'_s, C_{dc}, and i_o are the source voltage, the duty cycle, the dc-link voltage, the source current, modulated source current, dc-link capacitor, and the load current respectively. The transfer functions of the plants can be obtained using Laplace transform.

$$i_s(s) = \frac{V_{dc}}{sL_s} d_s(s) + \frac{V_{s(s)} - V_{dc}(s)}{sL_s} \quad (4)$$

$$V_{dc}(s) = \frac{1}{sC_{dc}} i'_s(s) - \frac{1}{sC_{dc}} i_o(s) \quad (5)$$

The first terms in (4) and (5) influence the dynamics of the system and the second terms are disturbances. The controllers are designed for the transfer functions shown in (6) and (7). The inner current loop is required to have faster response, as such the bandwidth ($\omega_{nc} = 2\pi f_{sw}/40$) of the current controller is selected to be much higher than the bandwidth of the dc-link voltage controller ($\omega_{nv} = 2\pi f_{sw}/400$).

The reduced transfer functions of the bidirectional converter and the dc-link can be expressed as in (6) and (7) in respective order.

$$G\_I(s) = \frac{i_s(s)}{d_s(s)} = \frac{V_{dc}}{sL_s} \quad (6)$$

$$G\_V(s) = \frac{V_{dc}(s)}{i'_s(s)} = \frac{1}{sC_{dc}} \quad (7)$$

The above expressions show that the dynamics of the converter is influenced by the power inductor and the dc-link capacitor. Since the transfer functions are first order systems, the control can be easily achieved using PI controllers by relating the general second order system (8) with the closed loop of the plant. The gain parameters of controllers are calculated analytically using the procedures presented in [20]. The general second order system is shown in (8).

$$G_{so}(s) = \frac{\omega^2_n \left(\frac{s}{z} + 1\right)}{s^2 + 2\zeta\omega_n s + \omega^2_n} \quad (8)$$

where ω_n is the undamped natural frequency, ζ is the damping factor, and z is the zero. The design specification ζ is chosen as 0.707 and ω_n is selected in accordance to the speed of the controllers needed. The closed-loop transfer function of the current plant (Tcl_I) and the PI controller can be expressed as:

$$Tcl\_I = \frac{i_s(s)}{i^*_s(s)} = \frac{\frac{K^c_p}{L_s}\left(s + \frac{K^c_i}{K^c_p}\right)}{s^2 + \frac{K^c_p V_{dc}}{L_s} s + \frac{K^c_i V_{dc}}{L_s}} \quad (9)$$

K^c_p and K^c_i are the proportional and integral gains of the current controller (PI). Comparing expression (9) with the general second order system in (8). The parameters can be calculated by choosing the required natural frequency and damping ratio.

$$K^c_p = \frac{2\omega_{nc}\zeta L_s}{V_{dc}} \quad (10)$$

$$K^c_i = \frac{\omega^2_{nc} L_s}{V_{dc}} \quad (11)$$

Likewise, the closed-loop transfer function (Tcl_V) of the dc-link can be written as:

$$Tcl\_V = \frac{V_{dc}(s)}{V^*_{dc}(s)} = \frac{\frac{K^v_p}{C_{dc}}\left(s + \frac{K^v_i}{K^v_p}\right)}{s^2 + \frac{K^v_p}{C_{dc}} s + \frac{K^v_i}{C_{dc}}} \quad (12)$$

Using the same approach, the PI gains for the voltage controller are calculated by (13) and (14).

$$K^v_p = 2\omega_{nv}\zeta C_{dc} \quad (13)$$

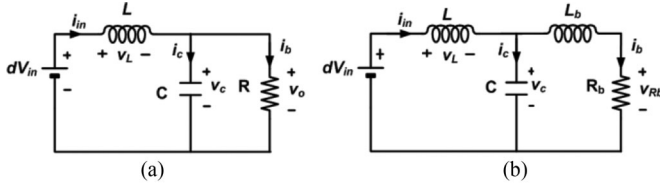$$K^v_i = \omega^2_{nv} C_{dc} \quad (14)$$

Fig. 4.   (a) Reduced average model of buck converter with Resistive load;
(b) Reduced average model of buck converter with auxiliary winding as load.

By referring to the main converter control layer depicted in Fig. 1, the reference current for the main winding is obtained from the dc-link controller. The dc-link controller input is the error signal obtained from the desired voltage reference and the actual dc-link voltage. The error signal is processed by the PI controller with gains designed in (13) and (14) to give the reference current across the power inductor. The current controller processes error signal obtained from the difference of the reference current and the actual measured current and accordingly provides control signals. This output is used as a reference signal to generate the PWM signals for controlling the power electronic switches of the bidirectional converter.

B. Auxiliary Converter Control Design

A buck converter is selected as an auxiliary converter for providing the controlled current for the VI. The specifications of the converter are presented in Table III.

In the actual implementation, the load is replaced by the auxiliary winding. The reduced average model of the buck converter without and with auxiliary winding as its load are depicted in Fig. 4(a) and (b), respectively.

The equations of the reduced average model of the buck converter, which is shown in Fig. 4(a), can be written as:

$$L\frac{di_{\text{in}}(t)}{dt} = dV_{\text{in}}(t) - v_c(t) \tag{15}$$

$$C\frac{dv_c(t)}{dt} = i_{\text{in}}(t) - \frac{v_c(t)}{R} \tag{16}$$

Combining (15) and (16), then replacing $v_c = i_b R$, and taking the Laplace transform. The output current to the control transfer function can be written as (17).

$$\frac{i_b(s)}{d(s)} = \frac{V_{\text{in}}}{RLCs^2 + Ls + R} \tag{17}$$

When the load is replaced by the auxiliary winding circuit, which consists of an inductance and a series resistance, the above model will be changed into a more complex third order system as shown in (18).

$$\frac{i_b(s)}{d(s)} = \frac{V_{\text{in}}}{L_b LCs^3 + R_b LCs^2 + Ls + R_b} \tag{18}$$

However, the third pole is very far from the dominant poles hence the system can be reduced. The characteristics of the designed buck converter is highly influenced by the auxiliary winding. Consequently, the third order model of the system is approximated by a first order transfer function of the auxiliary winding circuit.

The conventional PI controller is selected and the design of the control parameters is performed using the procedures used previously. The closed-loop transfer function can be written as:

$$\frac{i_b(s)}{i^*_b(s)} = \frac{\frac{K_p^b}{L_s}\left(s + \frac{K_i^b}{K_p^b}\right)}{s^2 + \frac{(R_b + K_p^b)}{L_b}s + \frac{K_i^b}{L_b}} \tag{19}$$

where K_p^b and K_i^b are the proportional and integral gain of the auxiliary winding current controller respectively. The superscript $*$ is to indicate a reference (set) value of a signal. In this study, the controller is designed based on ζ (0.707) and ω_n is selected to be 1/20 times the switching frequency in rad/s to make it much faster than the main winding current controller.

By comparing the denominators of (8) and (19), the gain parameters of the controller are determined as in (20) and (21).

$$K_i^b = 2\omega_{\text{nc}}\zeta L_b - R_b \tag{20}$$

$$K_i^b = \omega^2_{\text{nc}} L_b \tag{21}$$

Referring to the auxiliary converter control layer in Fig. 1, the reference current of the current controlled auxiliary converter is obtained from the control current estimator block. For practical implementation of the controllers in the microcontroller, Tustin approximation method is used for digital conversion.

C. Global Control Operation

As it is revealed in Fig. 1 the control layer consists of the main converter control layer and the auxiliary converter control layer. The first consists of the dc-link controller and the current controller, while the second one is composed of the reference current estimator block and the auxiliary current controller. The main winding reference current is obtained from the dc-link controller.

In the auxiliary converter control block, the auxiliary current estimator is determined from a series of tests. For several current levels in the main winding, the control current is varied in steps of 0.05 A until a minimum ripple current is noticed for each main current. Then the curve fitting approach is used to determine the control function (relationship) relating the auxiliary winding and main winding currents. This enables an automatic closed loop (integrated) control of the overall system. After obtaining the mathematical relationship between the two currents, the integrated closed loop system that consist of the closed loop of the main converter and the closed loop of the auxiliary converter with its current estimator block is implemented in a microcontroller. The curve, which shows the relationship between the two currents, is shown in Fig. 5.

As it is clearly shown, for currents less than 6.5 A, the auxiliary winding is idle, hence, the control current is zero. However, for currents greater than or equal to the saturation current, an appropriate control current is applied to the auxiliary winding in accordance to the curve shown in Fig. 5.
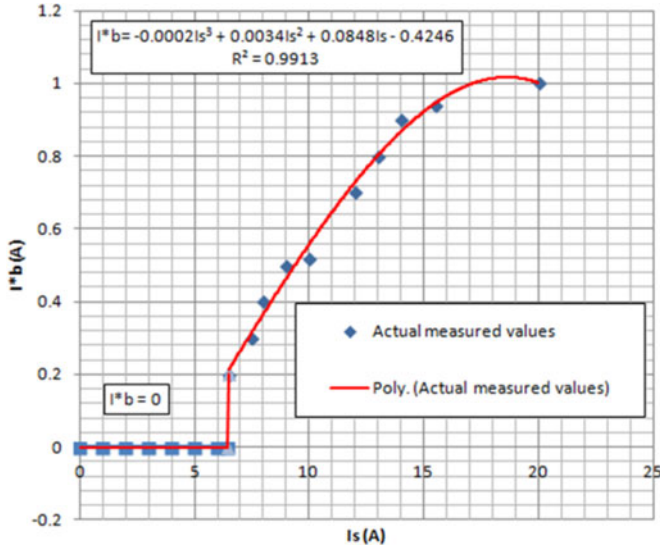
Fig. 5.   Auxiliary winding reference current and the main winding current relationship curve.

Fig. 6.   Experimental setup of VI-based converter test bench.

TABLE IV
RIPPLE VARIATIONS WITH THE INCREASE OF CURRENT

Duty Cycle	I_{srms} (A)	I_{savg} (A)	Peak to Peak RippleΔ_{i_s} (A)	Ripple (%)
0.50	3.94	3.77	1.6	42.44
0.52	3.96	3.94	1.76	44.67
0.58	6.3	6.24	3.6	57.69
0.60	7.79	7.7	3.8	62.34
0.62	8.81	8.25	6.8	82.42
0.63	9.39	9.22	8	86.77
0.64	11.5	11.3	9.8	86.73
0.65	12.8	12.2	11	90.16
0.70	17.78	17.2	15.65	91.00

IV. EXPERIMENTAL SETUP AND RESULTS

The experimental setup consists of a C-Class DC chopper IGBT topology (1200 V, 100 A) operating in continuous conduction mode powered by two batteries in parallel, a current controlled buck converter, power supplies, measuring instruments, RLC meter and C2000 launch pad Piccolo platform microcontroller. For interfacing the measurement signals to the microcontroller and the control signals to the IGBTs an interface PCB was manufactured. The conventional power inductor is replaced by the selected VI-prototype presented in Section II B. The buck converter is built in a PCB mounting approach and its controller is implemented in the same microcontroller. To emulate the dynamic behavior of the EV traction system, two batteries and a resistive load are used as a variable load. A 3.3 mF, 400 V capacitor is used as dc-link capacitor and a voltage sensor is used to measure its voltage. Two current sensors are also used for measuring the main winding current and the auxiliary winding current. As a small current variation in the auxiliary winding can influence the effective inductance of the main winding, a precision current sensor is selected. The experimental set up is shown in Fig. 6.

The experiments in this section are focused on the global system in order to clearly understand the effects and improvements due to the introduction of the VI to the bidirectional converter. For that, its characteristic is studied both without and with the activation of the auxiliary winding. As such, the main winding current is varied until the saturation current level is reached and beyond. As a result, it is found that operating the power inductor above the saturation limit leads to higher current ripples. This results in the heating of the switching devices and distortion in the current waveform, as expected by the theory. The experimental results for characterizing the ripple levels due to the variations of the main current are summarized in Table IV.

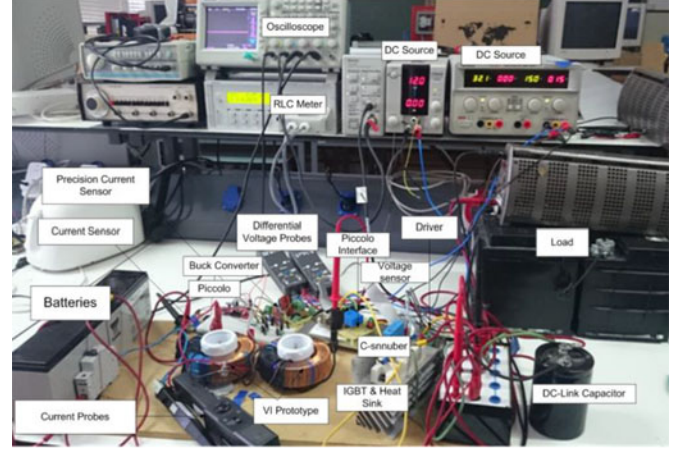It can be clearly shown that the increase of current in the main winding results in more ripple. Increasing the duty cycle from 0.50 to 0.70 increases the peak-to-peak current ripple significantly. For instance, for D = 0.65 and D = 0.70, the ratio of peak-to-peak current ripple reaches 90.16% and 91.00% respectively. Such a high ripple results in more losses, affecting the efficiency and performance of power converters. This describes the typical behavior of such converters for applications with a wide range of load variations, if the power inductor in the converter is pushed to operate in the saturation region.

After carefully analyzing the characteristics of the power inductor with the increase of current in the main winding, the auxiliary winding is activated and a controlled current is injected to it. This current helps in regulating the effective inductance of the main winding by changing the permeability of the magnetic core. For the last two cases in Table IV, a control current is applied in the auxiliary winding to quantify the amount of ripple improvements and the current handling capability of the power inductor. For D = 0.65, the amount of current ripple is 90.16%, when no control current is injected into the auxiliary winding. However, by injecting a control current of 0.75 A (Fig. 7(b)) and 1 A (Fig. 7(c)), the amount of current ripple can be reduced by 40.90 % and 38.20 % in respective order.

It is important to note in this case; the current waveforms show that injecting a control current in the auxiliary winding not only reduce the amount of current ripple but also enhance the current handling capability of the power inductor. In Fig. 7, the average current is twice the rated current of the power
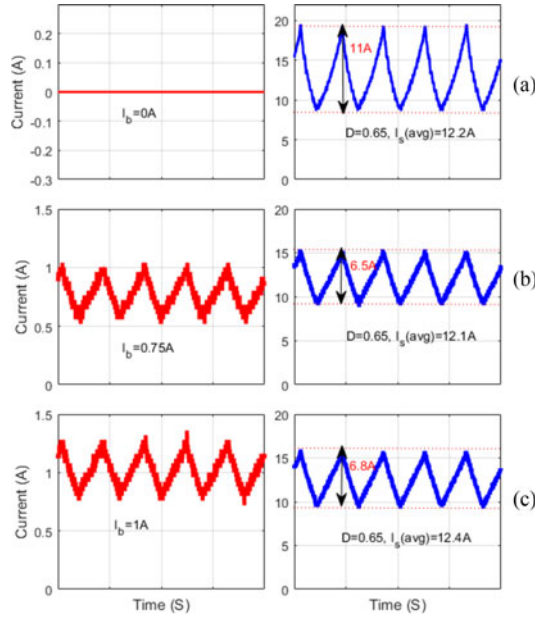
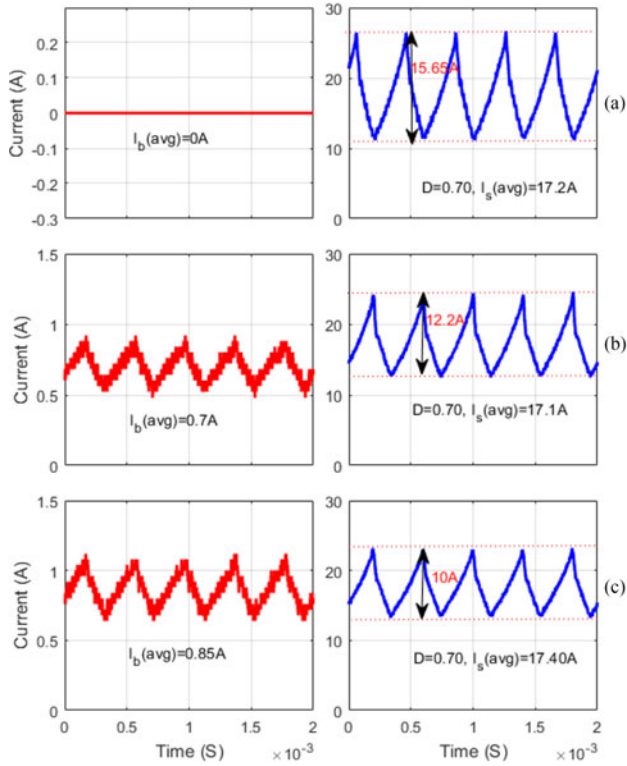Fig. 7. Experimental results for D = 0.65 with control current in the auxiliary winding.

Fig. 8. Experimental results for D = 0.70 with control current in the auxiliary winding.
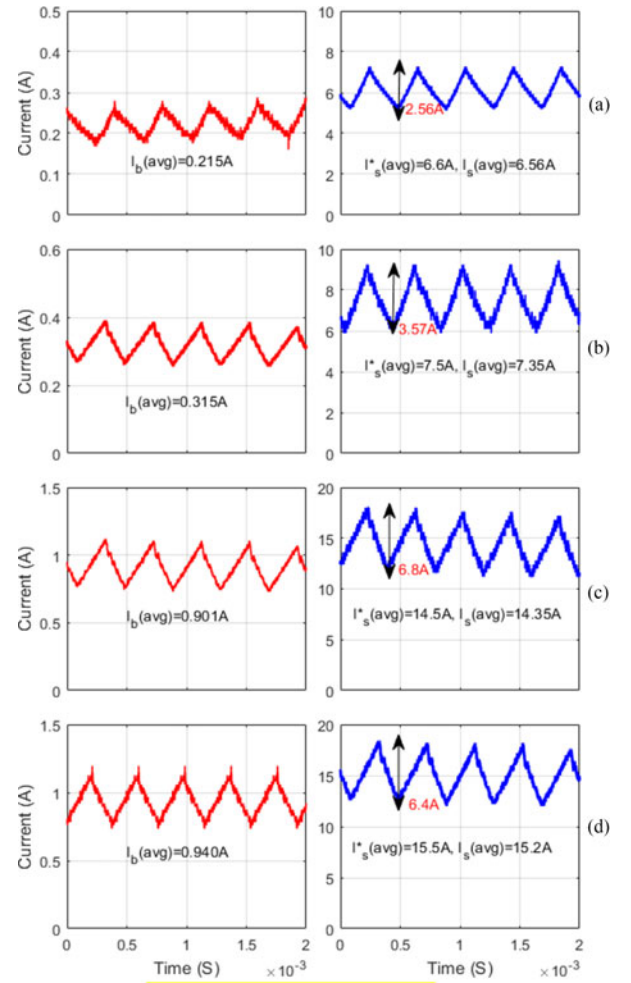

Fig. 9. Closed loop results.

0.70, a control current of 0.70 A and 0.85 A are applied and the current ripple in the main winding is reduced by 20% and 36% in respective order. In this case, the ripple current is reduced significantly, but as the level of current is much higher than the rated current of the power inductor, the power inductor operates in the saturation region. From the results shown in Fig. 8, the VI can be used with about 2.9 times the rated current of the power inductor. At these levels of current, the power inductor is saturated, but with the injection of a control current, its operating point can be forced to move from deep saturation to saturation region closer to the transition region. This leads to a significant current ripple reduction, resulting in the reduction of losses.

The injected auxiliary winding current pre-bias the magnetic core and helps in cancelling part of the main flux in the main winding that enables the magnetic core to operate in partial saturation. This operation regulates the effective permeability of the magnetic cores resulting in adjusting the inductance of the power inductor. This helps in the ripple control and enhances the current handling capability of the power inductor. Some of the experimental results of the integrated closed loop operation of the overall system (including now the auxiliary current level estimator) are presented in Fig. 9. In each plot, the auxiliary winding current and main converter current are shown

inductor. If no control current is applied, the power inductor is forced to operate in saturation region. Nonetheless, with a control current, the power inductor can be pushed to operate in partial saturation, which results in the current ripple control and improving the current handling capability of the power inductor. Similarly, as shown in Fig. 8(b) and (c), for the D =

in the left side and in the right side, respectively. As it can be clearly shown in Fig. 9, there is very slight difference between the measured current and the reference current, this is mainly due to the noisy nature of the current sensor used.

It can be also shown that the closed loop system provides better control of the current ripples. In Fig. 9(d), the main winding current is 15.2 A, which is 2.53 times higher than the rated current of the inductor. At this level of current, with the help of the integrated control, a controlled auxiliary winding is applied and the current ripple is kept 42.1%, which is much better than the open loop result with less main current (12.2 A) in Fig. 7. Furthermore, as it takes into considerations the current levels of the main winding, it provides precise regulation of the inductance and control of current ripples

V. Conclusion

This paper presents the viability of VI based bidirectional DC-DC converter for applications with a wide range of load variation such as EV. The conventional power inductor in DC-DC converter is replaced by VI in order to have better ripple control, enhanced current handling capability and adaptive control of the saturation level of a power inductor. To achieve the aforementioned goals, a low-cost, and low-power biasing circuit is built and a mathematical relationship that relates the auxiliary winding current with the levels of the main winding current is developed. The validity of the proposed VI, the biasing circuit and the improved DC-DC converter are verified through experimental tests. From the experimental results, it can be deduced that, with a small auxiliary winding current, the current handling capacity of a power inductor can be significantly improved. For currents twice the rated current, the ripple current is reduced from 11 A to 6.5 A, which is 40.90 % reduction. Similarly, for currents 2.9 times larger than the rated current, the current ripple is reduced from 15.65 A to 10 A (36.10 % decrease). It should be noted that for this level of current, the core is still in saturation, but the current ripple can still be reduced. Therefore, with the same core size the current handling capability is greatly improved, hence a remarkable step for core size miniaturization of magnetic components. The long-term plan of this work is to develop VI-based converters for EV applications and full-scale validation.

Acknowledgment

References

[1] F. Machado, J. P. F. Trovão, and C. H. Antunes, "Effectiveness of supercapacitors in pure electric vehicles using a hybrid metaheuristic approach," *IEEE Trans. Veh. Technol.*, vol. 65, no. 1, pp. 29–36, Jan. 2016.

[2] O. C. Onar, J. Kobayashi, D. C. Erb, and A. Khaligh, "A bidirectional high-power-quality grid interface with a novel bidirectional noninverted buck-boost converter for PHEVs," *IEEE Trans. Veh. Technol.*, vol. 61, no. 5, pp. 2018–2032, Jun. 2012.

[3] R. D. Castro, R. E. Araujo, J. P. F. Trovao, P. G. Pereirinha, P. Melo, and D. Freitas, "Robust DC-Link control in EVs with multiple energy storage systems," *IEEE Trans. Veh. Technol.*, vol. 61, no. 8, pp. 3553–3565, Oct. 2012.

[4] Y. Cho and J. S. Lai, "High-efficiency multiphase DC-DC converter for fuel-cell-powered truck auxiliary power unit," *IEEE Trans. Veh. Technol.*, vol. 62, no. 6, pp. 2421–2429, Jul. 2013.

[5] D. Han, J. Noppakunkajorn, and B. Sarlioglu, "Comprehensive efficiency, weight, and volume comparison of SiC- and Si-based bidirectional DC-DC converters for hybrid electric vehicles," *IEEE Trans. Veh. Technol.*, vol. 63, no. 7, pp. 3001–3010, Sep. 2014.

[6] M. S. Perdigão, J. P. F. Trovão, J. M. Alonso, and E. S. Saraiva, "Large-signal characterization of power inductors in EV bidirectional DC-DC converters focused on core size optimization," *IEEE Trans. Ind. Electron.*, vol. 62, no. 5, pp. 3042–3051, May 2015.

[7] Z. Dang and J. A. A. Qahouq, "Evaluation of high-current toroid power inductor with NdFeB magnet for DC-DC power converters," *IEEE Trans. Ind. Electron.*, vol. 62, no. 11, pp. 6868–6876, Nov. 2015.

[8] R. Lee, *Electronic Transformers and Circuits*. Hoboken, NJ, USA: Wiley, 1947.

[9] O. Hegazy, J. V. Mierlo, and P. Lataire, "Analysis, modeling, and implementation of a multidevice interleaved DC/DC converter for fuel cell hybrid electric vehicles," *IEEE Trans. Power Electron.*, vol. 27, no. 11, pp. 4445–4458, Nov. 2012.

[10] S. M. Ahsanuzzaman, T. McRae, M. M. Peretz, and A. Prodić, "Low-volume buck converter with adaptive inductor core biasing," in *Proc. 27th Annu. IEEE Appl. Power Electron. Conf. Expo.*, 2012, pp. 335–339.

[11] M. Hirakawa *et al.*, "High power dc/dc converter using extreme close-coupled inductors aimed for electric vehicles," in *Proc. Int. Power Electron. Conf.*, 2010, pp. 2941–2948.

[12] S. M. Dwari and L. Parsa, "A novel high efficiency high power interleaved coupled-inductor boost DC-DC converter for hybrid and fuel cell electric vehicle," in *Proc. 2007 IEEE Veh. Power Prop. Conf.*, 2007, pp. 399–404.

[13] W. H. Martinez and C. A. Cortes, "High power density interleaved DC-DC converter for a high performance electric vehicle," in *Proc. Workshop Power Electron. Power Qual. Appl.*, 2013, pp. 1–6.

[14] L. Po-Wa, L. Yim-Shu, D. K. W. Cheng, and L. Xiu-Cheng, "Steady-state analysis of an interleaved boost converter with coupled inductors," *IEEE Trans. Ind. Electron.*, vol. 47, no. 4, pp. 787–795, Aug. 2000.

[15] W. Li and X. He, "Review of nonisolated high-step-Up DC/DC converters in photovoltaic grid-connected applications," *IEEE Trans. Ind. Electron.*, vol. 58, no. 4, pp. 1239–1250, Apr. 2011.

[16] J. M. Alonso, M. S. Perdigão, J. Ribas, D. Gacio, and E. S. Saraiva, "Optimizing universal ballasts using magnetic regulators and digital control," *IEEE Trans. Ind. Electron.*, vol. 58, no. 7, pp. 2860–2871, Jul. 2011.

[17] A. S. Kislovski, "Quasi-linear controllable inductor," *Proc. IEEE*, vol. 75, no. 2, pp. 267–269, Feb. 1987.

[18] Y. Hu, L. Huber, and M. Jovanović, "Current-controlled variable inductor," U.S. Patent 8120457 B2, 2012.

[19] E. Rozanov and S. Ben-Yaakov, "A SPICE behavioral model for current-controlled magnetic inductors," in *Proc. 2004 23rd IEEE Conv. Elect. Electron. Eng. Israel*, 2004, pp. 338–341.

[20] R. Kadri, J. P. Gaubert, and G. Champenois, "An improved maximum power point tracking for photovoltaic grid-connected inverter based on voltage-oriented control," *IEEE Trans. Ind. Electron.*, vol. 58, no. 1, pp. 66–75, Jan. 2011.

Mebrahtom Woldelibanos Beraki (S'14) received the B.Sc. degree from the University of Asmara, Asmara, Eritrea, in 2008 and the M.Sc. degree from the University of Oviedo, Gijon, Spain, in 2015. He is currently working toward the Ph.D. degree in electrical engineering at the University of Sherbrooke, Sherbrooke, QC, Canada. His research interests include power electronics, electric vehicles, sustainable energy technologies, and grid integration of renewable energy sources and control.

João Pedro F. Trovão (S'08–M'13) was born in Coimbra, Portugal, in 1975. He received the M.Sc. and Ph.D. degrees in electrical engineering from the University of Coimbra, Coimbra, Portugal, in 2004 and 2013, respectively. From 2000 to 2014, he was a Teaching Assistant and an Assistant Professor in the Polytechnic Institute of Coimbra–Coimbra Institute of Engineering (IPC–ISEC), Coimbra, Portugal. Since 2014, he has been a Professor with the Department of Electrical Engineering and Computer Engineering, University of Sherbrooke, Sherbrooke, QC, Canada, where he holds the Canadian Research Chair position in efficient electric vehicles with Hybridized Energy Storage Systems. His research interests include areas of electric vehicles, hybridized energy storage systems, energy management, and rotating electrical machines. He was the General Co-Chair and the Technical Program Committee Co-Chair of the 2014 IEEE Vehicle Power and Propulsion Conference, as well as the Award Committee Member for the 2015 and the 2016 IEEE Vehicle Power and Propulsion Conferences. He is the Technical Program Committee Co-Chair of the 2017 IEEE Vehicle Power and Propulsion Conference. He was a Guest Editor for the Special Issue of IET Electrical Systems in Transportation on Energy Storage and Electric Power Sub-Systems for Advanced Vehicles. He is currently a Guest Editor for the Special Issue of IEEE TRANSACTIONS ON VEHICULAR TECHNOLOGY on Electric Powertrains for Future Vehicles.

Marina S. Perdigão (S'06–M'12) was born in Coimbra, Portugal, in 1978. She received the M.Sc. and Ph.D. degrees in electrical engineering from the University of Coimbra, Coimbra, Portugal, in 2004 and 2012, respectively. From 2006 to 2012, she conducted her Ph.D. work with the University of Coimbra in cooperation with the University of Oviedo, Oviedo, Spain. Since 2002, she has been with the Polytechnic Institute of Coimbra–Coimbra Institute of Engineering, Coimbra, first as a Teaching Assistant and then as an Assistant Professor since 2012. She has been a Researcher in the Instituto de Telecomunicações, Coimbra, Portugal, since 2001. She is the co-author of more than 50 journal and conference publications, including 13 publications in highly referenced journals. Her research interests include high-frequency electronic ballasts, discharge lamp modelling, high-frequency switching converters, resonant converters, dc–dc converters, power electronics for renewable energies, IPT, and computer simulation applications. She received the best paper award of the 2009 IEEE International Symposium on Industrial Electronics and was awarded by the Industrial Lighting and Display Committee of the IEEE Industry Applications Society a First Prize Paper for the technical competence displayed. She collaborates as a transactions Paper Reviewer as a IEEE Member.

Maxime R. Dubois (M'99) received the B.Sc. degree in electrical engineering from the Université Laval, Québec, QC, Canada, in 1991, and the Ph.D. degree (*cum laude*) from Delft University of Technology, Delft, The Netherlands, in 2004. Between 1993 and 1999, he has worked in the industry as a Power Electronics Engineer. Between 2004 and 2011, he has been with the Université Laval. Since 2011, he has been an Associate Professor in the Department of Electrical Engineering, University of Sherbrooke, Quebec, QC, Canada. He is the founder of Eocycle Technologies, Inc., a company specialized in the development of TFPM. He is also the Founding Professor of the company AddEnergie Technologies. His research interests include electrical machines and power electronics applied to the field of wind energy, energy storage, and electric vehicles. He was the Technical Program Committee Chair of the 2015 IEEE Vehicle Power and Propulsion Conference and a Guest Editor for the Special Issue of IET Electrical Systems in Transportation on Design, Modeling, and Control of electric Vehicles.